Sub-Harmonic Resonance in Three-Dimensional Boundary Layer Flow

JC Chen* and Weijia Chen

***Abstract*—Sub-harmonic resonance in zero pressure gradient three-dimensional boundary layer flow occurs in the classical N-type pathway of turbulence transition. Three-dimensionality incurs exorbitant computational demands on the numerical simulations. Imposition of a spectral method and a non-uniform grid countervails the impractical computational demands. Eigenvalue analysis ascertains ranges of stability of the numerical method. Validation of the numerical method versus the three-dimensional OS equation avers confidence in the accuracy of the model. Numerical realizations of the generation, amplification, and interaction of two- and three-dimensional sub-harmonic waves agree qualitatively with classical experiments.**

***Index Terms*—sub-harmonic resonance, spectral method, non-uniform grid, three-dimensional boundary layer flow**

I. Introduction

The classical work, Schubauer and Skramstad, 1947 [1], conducts a famous experiment to examine the topic of boundary layer turbulence transition. The experiment entails a vibrating ribbon that is placed at the base of the inlet to a flow channel and acts to introduce perturbations into the flow. The perturbations evolve into disturbance waves known as Tollmien–Schillichting (TS) waves that travel downstream. As the disturbance waves propagate downstream, they will begin to interact with one another in progressive stages of transition towards flow turbulence. Initially, the wave interactions are linear in the linear instability stage [2]. Further downstream, the wave interactions become nonlinear. The nonlinear interactions spawn a secondary instability in the flow. The secondary instability eventually becomes unsustainable and break down into turbulence. The stages of transition up to linear instability are well-understood presently. The linear wave interactions can be described accurately with the Orr-Sommerfeld (OS) equation of linear stability theory. Chen and Chen, 2010 [3] proffers a scholastic study of the linear stage of turbulence transition. However, once the waves undergo nonlinear interactions, the transition phenomenon becomes mysterious and is the subject of much cerebation.

A subsequent classical work, Klebanoff, *et al.*, 1962 [4], would shed illuminating insight into the nonlinear stage of transition. As transition to turbulence can occur via multiple pathways, Klebanoff, *et al.*, 1962 [4] studies the pathway that has come to bear the namesake of its author, K-type transition. When the amplitude of the initial perturbation exceeds 1% of the mean flow, the K-type transition mechanism activates to induce an explosive amplification of waves leading to breakdown into turbulence. Klebanoff, *et al.*, 1962 [4] observes definitive and reproducible behavior of nonlinear wave interactions beginning with the formation of the first set of waves from the perturbation known as the fundamental waves. The fundamental wave exercises a fecundity that begets second and third harmonics of successively higher wave frequencies. The harmonics would then cluster in wave packets as they traverse downstream. Within the packets, the waves interact and synchronize. The phase synchronization of the waves results in explosive spikes in the observed wave oscillations. These observations have become bespoke signature features of nonlinear turbulence transition [4].

Additional classical works would ensue. Kachanov and Levchenko, 1984 [5] and Kachanov, 1994 [6] reveal another possible pathway towards turbulence called the N-type transition. The N-type transition facilitates a more controlled pathway to turbulence, evoked by a lower amplitude of the initial disturbance than K-type transition. As such, the N-type transition transpires with measurably exponential amplification of waves as contrasted with the incontinent explosion in the K-type. Also, the N-type transition generates harmonics of lower frequencies than the K-type. The N-type wave interactions are termed sub-harmonic resonance that involves the initial TS disturbance waves of a given frequency β_1 and subsequently generated sub-harmonic waves with frequencies $\beta_{1/2} \approx \beta_1/2$. For more details, Herbert, 1988 [7] offers an excellent review of the nonlinear transition stage.

Chen, 2009 [8], Chen and Chen, 2010 [3] Chen and Chen, 2011 [9], Chen and Chen, 2011 [10], Chen and Chen, 2012 [11], Chen and Chen, 2012 [12], Chen and Chen, 2009 [2], Chen and Chen, 2010 [13], Chen and Chen, 2011 [14], and Chen and Chen, 2011 [15] respectfully anthologize its study of boundary layer turbulence transition.

II. Three Dimensionality

During the transition towards turbulence, the generated waves acquire a three-dimensional characteristic. The formation of three-dimensional waves represents a key development in turbulence transition. Saric, *et al.*, 2003 [16] explains that the three-dimensional waves arise from crossflow and centrifugal instabilities occurring in flow regions with pressure gradients. The three-dimensional nature of the flow is the critical element that leads to rapid

Manuscript received 23 September, 2011; supported by Ministry of Education Grant RG 4/07.

*JC Chen, Corresponding Author, Nanyang Technological University, School of Civil and Environmental Engineering, Singapore (phone: +65 6790-5273; fax: +65 6790-5273; e-mail: jimchen@ntu.edu.sg).

Weijia Chen, Nanyang Technological University, School of Civil and Environmental Engineering, Singapore.

ISBN: 978-988-19251-9-0
ISSN: 2078-0958 (Print); ISSN: 2078-0966 (Online)

generation of additional harmonics and their subsequent explosive or exponential amplification. Orszag and Patera, 1983 [17] notes that, during wave interactions, the two-dimensional waves are unstable to the presence of even infinitesimal three-dimensional waves and will amplify exponentially from the encounter. Orszag and Patera, 1983 [17] systematically illustrates that the combination of vortex stretching and tilting terms in the governing Vorticity Transport Equation accelerates the growth of waves. Both vortex stretching and tilting are required to produce the accelerated growth of waves [17]. Both are three-dimensional phenomena and thus, concurringly underline the important role of three-dimensionality in turbulence transition. Reed and Saric, 1989 [18] and Herbert, 1988 [7] offer excellent reviews of the mechanisms that cause the formation of three-dimensional waves.

Three-dimensional flows carve a frontier of great interest in cutting-edge fluid dynamics research. However, numerical visualization of three-dimensional waves incurs vast computational demands. The computational demands exponentially reach impractical levels for even typical turbulent flow conditions. Therefore, easing computational demands to within practical limits poses a mandate of utmost importance. Spectral methods offer such a reprieve.

III. Problem Definition

A. Flow Domain

Figure 1 depicts the flow problem as the classical three-dimensional boundary layer flow problem of Schubauer and Skramstadt, 1947 [1]. A blowing and suction strip generates the disturbances. The spanwise z-direction covers one disturbance wavelength λ_z. A buffer domain before the outflow boundary ramps down the disturbances to prevent wave reflection [9, 13].

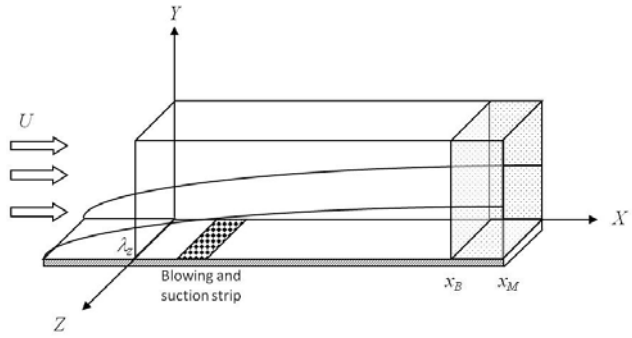

Fig. 1. Schematic of the flow domain.

B. Governing Equations

Non-dimensional variables are used. They are related to their dimensional counterparts, denoted by bars, as follows:

$$Re = \frac{\overline{U}_\infty \overline{L}}{\overline{\nu}},\ x = \frac{\overline{x}}{\overline{L}},\ y = \frac{\overline{y}\sqrt{Re}}{\overline{L}}, \tag{1a}$$

$$t = \frac{\overline{U}_\infty \overline{t}}{\overline{L}},\ u = \frac{\overline{u}}{\overline{U}_\infty},\ v = \frac{\overline{v}\sqrt{Re}}{\overline{U}_\infty},\ \text{and}\ w = \frac{\overline{w}}{\overline{U}_\infty} \tag{1b}$$

where the characteristic length $\overline{L} = 0.05$ m, freestream velocity $\overline{U}_\infty$ = 30 m/s, kinematic viscosity $\overline{\nu}$ = 1.5 × 10^{-5} m^2/s, Re is the Reynolds number, u, v, and w are the streamwise, transverse, and spanwise flow velocities.

The total flow velocity and vorticity $(V,\ \Omega)$ comprise a steady two-dimensional base flow $(V_B,\ \Omega_B)$ and an unsteady three-dimensional disturbance flow $(V',\ \Omega')$ [19, 20]:

$$V(t,x,y,z) = V_B(x,y,z) + V'(t,x,y,z), \tag{2}$$

$$\Omega(t,x,y,z) = \Omega_B(x,y,z) + \Omega'(t,x,y,z), \tag{3}$$

$$V_B = \{u_B, v_B, 0\},\ \Omega_B = \{0, 0, \omega_{z_B}\}, \text{and} \tag{4}$$

$$V' = \{u', v', w'\},\ \Omega' = \{\omega_x', \omega_y', \omega_z'\}. \tag{5}$$

The governing equations for the disturbance flow is the Vorticity Transport Equation [19, 20]:

$$\frac{\partial \omega_x'}{\partial t} + \frac{\partial a}{\partial y} - \frac{\partial c}{\partial z} = \frac{1}{Re}\frac{\partial^2 \omega_x'}{\partial x^2} + \frac{\partial^2 \omega_x'}{\partial y^2} + \frac{1}{Re}\frac{\partial^2 \omega_x'}{\partial z^2}, \tag{6}$$

$$\frac{\partial \omega_y'}{\partial t} - \frac{\partial a}{\partial x} + \frac{\partial b}{\partial z} = \frac{1}{Re}\frac{\partial^2 \omega_y'}{\partial x^2} + \frac{\partial^2 \omega_y'}{\partial y^2} + \frac{1}{Re}\frac{\partial^2 \omega_y'}{\partial z^2}, \tag{7}$$

$$\frac{\partial \omega_z'}{\partial t} + \frac{\partial c}{\partial x} - \frac{\partial b}{\partial y} = \frac{1}{Re}\frac{\partial^2 \omega_z'}{\partial x^2} + \frac{\partial^2 \omega_z'}{\partial y^2} + \frac{1}{Re}\frac{\partial^2 \omega_z'}{\partial z^2}, \tag{8}$$

$$a = v'\omega_x' - u'\omega_y' + v_B{}'\omega_x' - u_B\omega_y', \tag{9}$$

$$b = w'\omega_y' - v'\omega_z' + v_B\omega_z' + v'\omega_{z_B}, \tag{10}$$

$$c = u'\omega_z' - w'\omega_x' + u_B\omega_z' + u'\omega_{z_B}, \text{and} \tag{11}$$

$$\omega_x' = \frac{1}{Re}\frac{\partial v'}{\partial z} - \frac{\partial w'}{\partial y},\ \omega_y' = \frac{\partial w'}{\partial x} - \frac{\partial u'}{\partial z},\ \omega_z' = \frac{\partial u'}{\partial y} - \frac{1}{Re}\frac{\partial v'}{\partial x}. \tag{12}$$

In addition, there is a set of Poisson's equations [19, 20]:

$$\frac{\partial^2 u'}{\partial x^2} + \frac{\partial^2 u'}{\partial z^2} = -\frac{\partial \omega_y'}{\partial z} - \frac{\partial^2 v'}{\partial x \partial y}, \tag{13}$$

$$\frac{1}{Re}\frac{\partial^2 v'}{\partial x^2} + \frac{\partial^2 v'}{\partial y^2} + \frac{1}{Re}\frac{\partial^2 v'}{\partial z^2} = \frac{\partial \omega_x'}{\partial z} - \frac{\partial \omega_z'}{\partial x}, \text{and} \tag{14}$$

$$\frac{\partial^2 w'}{\partial x^2} + \frac{\partial^2 w'}{\partial z^2} = \frac{\partial \omega_y'}{\partial x} - \frac{\partial^2 v'}{\partial y \partial z}. \tag{15}$$

Finally, the continuity equation completes the set:

$$\frac{\partial u'}{\partial x} + \frac{\partial v'}{\partial y} + \frac{\partial w'}{\partial z} = 0. \tag{16}$$

Zero pressure gradient (ZPG) boundary layer flow serves as the base flow. The solution procedure begins by solving the two-dimensional steady base flow followed by the three-dimensional disturbance flow. Chen and Chen, 2011 [9] copiously detail this solution algorithm.

C. Boundary Conditions

Inflow Boundary Condition

The inflow boundary introduces no disturbances; hence, u', v', w', ω_x', ω_y', and ω_z' along with their first and second derivatives are all zero there.

Freestream Boundary Condition

Assuming potential flow at the freestream boundary, the vorticity is zero there:

ISBN: 978-988-19251-9-0
ISSN: 2078-0958 (Print); ISSN: 2078-0966 (Online)

$$\omega_x' = 0,\ \frac{\partial \omega_x'}{\partial y} = 0,\ \frac{\partial^2 \omega_x'}{\partial y^2} = 0, \quad (17)$$

$$\omega_y' = 0,\ \frac{\partial \omega_y'}{\partial y} = 0,\ \frac{\partial^2 \omega_y'}{\partial y^2} = 0, \quad (18)$$

$$\omega_z' = 0,\ \frac{\partial \omega_z'}{\partial y} = 0,\ \frac{\partial^2 \omega_z'}{\partial y^2} = 0, \text{ and} \quad (19)$$

$$\frac{\partial v'}{\partial y} = -\frac{\alpha^*}{\sqrt{Re}} v'. \quad (20)$$

The parameter v' decays much slower, and so its wall-normal derivative remains appreciable with a prescribed wave number of α^*. The other parameters u' and w' would result from the solution of the governing equations.

Wall Boundary Condition

The boundary conditions at the wall are:

$$u' = 0, \quad (21)$$

$$v' = 0,\ \frac{\partial v'}{\partial y} = 0, \quad (22)$$

$$w' = 0, \quad (23)$$

$$\frac{\partial^2 \omega_x'}{\partial x^2} + \frac{\partial^2 \omega_x'}{\partial z^2} = -\frac{\partial \omega_y'}{\partial x \partial y} + \frac{\partial}{\partial z}\left(\frac{1}{Re}\frac{\partial^2 v'}{\partial x^2} + \frac{\partial^2 v'}{\partial y^2} + \frac{1}{Re}\frac{\partial^2 v'}{\partial z^2}\right), \quad (24)$$

$$\omega_y' = 0, \text{ and} \quad (25)$$

$$\frac{\partial^2 \omega_z'}{\partial x} = \frac{\partial \omega_x'}{\partial z} - \left(\frac{1}{Re}\frac{\partial^2 v'}{\partial x^2} + \frac{\partial^2 v'}{\partial y^2} + \frac{1}{Re}\frac{\partial^2 v'}{\partial z^2}\right). \quad (26)$$

Correct definition of the wall boundary conditions remains a hotly contested matter. Problematic issues include the need to preserve continuity and vorticity. Chen and Chen, 2010 [3] engage in a tendentious intellection of the issue of defining the wall boundary condition.

The blowing and suction strip shown in Fig. 1 generates disturbances in spectral space according to:

$$\hat{v}_k = A_k f(x)\sqrt{Re}\sin(\beta_k t), \quad (27)$$

$$f(x) = \begin{cases} 24.96\xi^6 - 56.16\xi^5 + 31.2\xi^4 \\ -24.96\xi^6 + 56.16\xi^5 - 31.2\xi^4 \end{cases}, \quad (28)$$

$$\xi = \frac{x - x_1}{x_{st} - x_1} \quad x_1 < x < x_{st} \text{ for the first case, and} \quad (29)$$

$$\xi = \frac{x_1 - x}{x_2 - x_{st}} \quad x_{st} < x < x_2 \text{ for the second case} \quad (30)$$

where k = 0 or 1, A_k the disturbance amplitude A_k = 1.0 × 10^{-4}, and the disturbance frequency β_k = 10.0. The Fourier modes k = 0 and 1 correspond to the two- and three-dimensional disturbances, respectively.

Outflow Boundary Condition

A buffer domain located at $x = x_B$ prior to the outflow boundary at $x = x_M$ ramps down the flow disturbances with ramping function:

$$T(L_b) = \frac{0.9778 + 1.3074\cos(\pi L_b) + 0.33187\cos(2\pi L_b) + 0.0022278\cos(3\pi L_b)}{1 + 0.63707\cos(\pi L_b) + 0.17261\cos(\pi L_b)} \text{ with} \quad (31)$$

$$L_b = \frac{x_B - x}{x_B - x_M}. \quad (32)$$

Spanwise Boundary Condition

The spanwise boundaries located at z = 0 and $z = \lambda_z$ implement periodic boundary conditions where all disturbance flow parameters and their derivatives at z = 0 are equal to their counterparts at $z = \lambda_z$.

IV. Spectral Method

Spectral methods offer the advantages of exponential convergence, numerical accuracy, and computational efficiency. They have demonstrated superior performance to finite difference methods [21]. Spectral methods approximate the solution to a given set of governing equations, for example, by assuming the solution be a Fourier series or Chebyshev polynomials [21]. In contrast, finite difference methods approximate the original governing equations and then seek to solve the approximate problem. Spectral methods are especially suited for problems with periodic boundary conditions, which in this study occurs at the spanwise boundaries. This study uses a Fourier series approximation for the solution [19, 20, 22]:

$$f'(x,y,z,t) = \sum_{k=-K}^{K} F_k(x,y,t)\exp(Ik\gamma_k z) \quad (33)$$

where f' is a flow variable of interest such as the velocity, $F_k(x,y,t)$ are the Fourier amplitudes, spanwise wave number $\gamma_k = 2\pi k/\lambda_z$, and λ_z is the largest spanwise wavelength of flow disturbances. The mode F_k is the complex conjugate of F_{-k}, so the governing equations and boundary conditions can be transformed to K+1 equations and boundary conditions in the two-dimensional x-y plane.

For cases with symmetric flow, the Fourier expansion can be compacted to sines and cosines separately as [19, 20, 22]:

$$(u', v', \omega_z', b, c) = \sum_{k=0}^{K} (\hat{u}_k', \hat{v}_k', \hat{\omega}_{zk}', B_k, C_k)\cos(\gamma_k z) \quad (34)$$

$$(w', \omega_x', \omega_y', a) = \sum_{k=1}^{K} (\hat{w}_k', \hat{\omega}_{xk}', \hat{\omega}_{yk}', A_k)\sin(\gamma_k z). \quad (35)$$

The parameters u', v', ω_z', b, and c are symmetric; w', ω_x', ω_y', and a are anti-symmetric. This compaction requires the simulation of half of the wavelength, $\lambda_z/2$, hence, reduces computational demands by half [19, 20, 22].

The governing equations in spectral representation are:

$$\frac{\partial \hat{\omega}_{xk}'}{\partial t} + \frac{\partial A_k}{\partial y} + \gamma_k C_k = \frac{1}{Re}\frac{\partial^2 \hat{\omega}_{xk}'}{\partial x^2} + \frac{\partial^2 \hat{\omega}_{xk}'}{\partial y^2} - \frac{\gamma_k^2}{Re}\hat{\omega}_{xk}', \quad (36)$$

$$\frac{\partial \hat{\omega}_{yk}'}{\partial t} - \frac{\partial A_k}{\partial x} - \gamma_k B_k = \frac{1}{Re}\frac{\partial^2 \hat{\omega}_{yk}'}{\partial x^2} + \frac{\partial^2 \hat{\omega}_{yk}'}{\partial y^2} - \frac{\gamma_k^2}{Re}\hat{\omega}_{yk}', \quad (37)$$

$$\frac{\partial \hat{\omega}_{zk}'}{\partial t} + \frac{\partial C_k}{\partial x} - \frac{\partial B_k}{\partial y} = \frac{1}{Re}\frac{\partial^2 \hat{\omega}_{zk}'}{\partial x^2} + \frac{\partial^2 \hat{\omega}_{zk}'}{\partial y^2} - \frac{\gamma_k^2}{Re}\hat{\omega}_{zk}', \quad (38)$$

$$\frac{1}{Re}\frac{\partial^2 \hat{v}_k'}{\partial x^2} + \frac{\partial^2 \hat{v}_k'}{\partial y^2} - \frac{\gamma_k^2}{Re}\hat{v}_k' = \gamma_k \hat{\omega}_{xk}' - \frac{\partial \hat{\omega}_{zk}'}{\partial x}, \quad (39)$$

$$\frac{\partial^2 \hat{w}_k'}{\partial x^2} - \gamma_k^2 \hat{w}_k' = \frac{\partial \hat{\omega}_{yk}'}{\partial x} + \gamma_k \frac{\partial \hat{v}_k'}{\partial y}, \text{ and} \quad (40)$$

$$\frac{\partial^2 \hat{u}_k'}{\partial x^2} - \gamma_k^2 \hat{u}_k' = -\gamma_k \hat{\omega}_{yk}' - \frac{\partial^2 \hat{v}_k'}{\partial x \partial y}. \quad (41)$$

ISBN: 978-988-19251-9-0
ISSN: 2078-0958 (Print); ISSN: 2078-0966 (Online)

V. Overall Numerical Method

The present study uses a spectral Fourier method in the spanwise direction. By that, imagine the flow domain shown in Fig. 1 to be divided into a series of x-y planes. For each x-y plane, the governing equations are given according to Eqs. (36) to (41). Each x-y plane would then need its numerical discretization. The spatial discretization uses 12th-order Combined Compact Difference (CCD) schemes. The temporal discretization uses a 4th-order 5-6 alternating stages Runge-Kutta (RK) scheme. Chen and Chen, 2011 [10], Chen and Chen, 2011 [9], and Chen and Chen, 2012 [12] comprise a graphomanic series on the development of these numerical methods.

VI. Non-Uniform Grid

A. Computational Efficiency

Since the numerical realization of turbulence transition exerts impractically onerous computational demands, one would do well to preserve computational resources as much as possible. One method of conservation uses non-uniform grids that concentrate the computational resolution in regions of interest and relax to coarse resolutions in regions of less relevance. For the case of boundary layer turbulence transition, this entails using very fine grids near the wall where the transition process occurs and gradually coarsening the grid with increasing distance away from the wall. In so doing, the precious resource of computational capacity would be allocated with maximum utility.

Furthermore, micro-scaled wave interactions in turbulence transition can be easily distorted by numerical errors. So, high-order numerical methods would seem to be a logical remedy to control the errors. However, the use of high-order numerical methods presents an additional issue at the wall boundary. To properly close a high-order numerical method, the appropriate boundary scheme would generally be at least one order lower than the numerical scheme in the interior domain, in order to prevent numerical instability [23]. The difference in orders between the interior and boundary schemes widens with increasing order of the numerical method [23]. So, even when using a high-order numerical method, the overall order of the numerical method would be diluted by the need for lower-order boundary schemes that poses a threat to the numerical stability [23]. One means to preserve numerical stability of high-order methods at the boundary and combat the dilutive effects of lowering the order of the boundary scheme implements non-uniform grids that concentrate fine grid spacing near the wall. The solution would first generate a non-uniform grid and then derive a numerical method with coefficients bespoke to the non-uniform grid [23].

B. Non-Uniform Grid Generation

The non-uniform grid is generated in the wall-normal y-direction using piecewise functions:

$$y = y_c\left(1+\frac{\operatorname{asin}\left(-\alpha_g\cos\left(\frac{\pi i}{2c}\right)\right)}{\operatorname{asin}(-\alpha_g)}\right) \quad \text{for} \quad 0 \le i \le c \tag{42}$$

$$y = y_c + (y_c - y_{c-1})\left(\frac{\beta_g^{(i-c)}-1}{\beta_g-1}\right) \quad \text{for } c+1 \le i \le n \tag{43}$$

where α_g and β_g are the grid stretching parameters and c is the index for a designated node point where the two piecewise functions meet.

C. Numerical Scheme Bespoke to Non-Uniform Grid

The numerical scheme would be derived bespoke to the non-uniform grid. High-order combined compact difference (CCD) schemes provide the advantages of accuracy of simulations and control of numerical errors. The CCD scheme combines the discretization for the function, f, its first derivative, F, and second derivative, S, with a, b, and c as the coefficients of the scheme and h as the grid size:

$$h\sum_{j=j_1}^{j_2} a_{1,j}F_{i+j} + h^2\sum_{j=j_1}^{j_2} b_{1,j}S_{i+j} + \sum_{j=j_1}^{j_2} c_{1,j}f_{j+j} = 0 \tag{44}$$

$$h\sum_{j=j_1}^{j_2} a_{2,j}F_{i+j} + h^2\sum_{j=j_1}^{j_2} b_{2,k}S_{i+j} + \sum_{j=j_1}^{j_2} c_{2,j}f_{i+j} = 0. \tag{45}$$

The coefficients of the CCD scheme are derived using Lagrange polynomial interpolation. The Lagrange polynomial interpolation of a function $y(x)$ is [23]:

$$y(x) = \sum_{i=1}^{n} l_i(x)f(x_i) \tag{46}$$

where $l_i(x)$'s are Lagrange basis polynomials [23]:

$$l_i(x) = \prod_{j=1, j\neq i}^{n} \frac{(x-x_j)}{(x_i-x_j)}. \tag{47}$$

The Lagrange polynomial interpolation can be extended to include higher-order derivatives [23]:

$$y(x) = \sum_{d=0}^{D}\sum_{i\in I_n}\rho_{d,i}(x)f^{(d)}(x_i) + \sum_{i\in I_m} r_i(x)f(x_i) \tag{48}$$

where $f^{(d)}(x_i)$ denotes the Dth-order derivative of the function $f(x_i)$, I_n is the set of points defining $f^{(d)}(x_i)$ up to the Dth-order derivative, I_m is the set of points defining only the function values of $f(x_i)$, and $\rho_{d,i}(x)$ and $r_i(x)$ are additional interpolation polynomials. The numerical schemes can be derived by differentiating Eq. (48) D times to obtain the expressions for $y^{(p)}(x)$ as [23]:

$$y^{(p)}(x) = \sum_{d=0}^{D}\sum_{i\in I_n}\rho_{d,i}^{(p)}(x)f^{(d)}(x_i) + \sum_{i\in I_m} r_i^{(p)}(x)f(x_i) \tag{49}$$

for p =1, 2, … , D. The coefficients of the scheme are derived from Eq. (49). In this study, the numerical scheme derived is a 12th-order 5-point non-uniform CCD scheme. The concomitant boundary schemes are 10th- and 11th-order.

VII. Stability of Numerical Method

With the objective of customizing the numerical method to a non-uniform grid for strengthening numerical stability, a logical evaluation of the numerical method would consider its ranges of stability. The stability of a numerical method entails two facets, the temporal and spatial discretizations. Both aspects must be numerically stable. Mathematical theory decrees that the properties of the eigenvalues of a spatial discretization define its range of numerical stability [24]. The eigenvalue analysis begins with applying the numerical method, in this case, a 12th-order 5-point non-uniform CCD scheme with 10th and 11th-order boundary schemes, to a reference governing equation, the classical one-dimensional convective diffusion equation. The theory mandates that the real part of the eigenvalue of the numerical discretization must be negative to ensure stability.

ISBN: 978-988-19251-9-0
ISSN: 2078-0958 (Print); ISSN: 2078-0966 (Online)

For the temporal discretization, the theory examines its amplification factor [24]. A temporal discretization will be stable if the absolute value of the amplification factor is less than one. Since the temporal discretization integrates the spatial discretization over time, the amplification factor is a function of the eigenvalue. This linkage allows for concurrent examination of the stabilities of both discretizations. The overall stability condition would require first that the real part of the eigenvalue be negative. Next, of these eigenvalues, ones that limit the amplification factor to less than one would be further selected.

Applying this two-step analysis to the one-dimensional convective diffusion equation indeed yields a set of eigenvalues for which the numerical method will remain stable, as depicted in Fig. 2. The stability of the numerical method when applied to this reference case provides indications as to how it will fare on the actual flow problem.

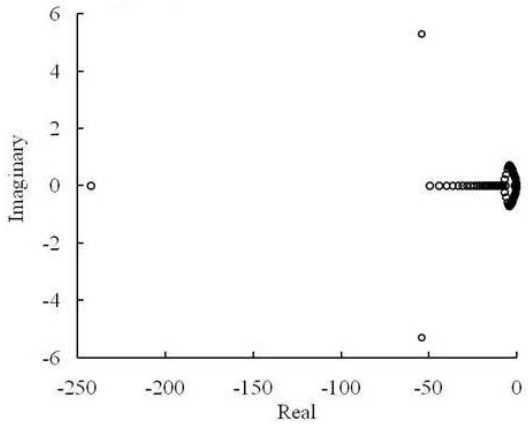

Fig. 2. Stability range of eigenvalues.

VIII. Validation of Numerical Method

The stable numerical method then must be validated for accuracy. An accurate numerical model would agree well with the Orr-Sommerfeld (OS) equation of linear stability theory. Figure 3 affirms agreement amongst the present study, three-dimensional OS equation, and numerical study of Fasel, *et al.*, 1990 [25] for the downstream amplification rate α_i of the disturbance velocity u':

$$\alpha_i = \frac{d}{dx}\ln(f') \tag{50}$$

where f' is the flow variable of interest. Similar results hold for v' and w'. Figure 4 asserts further averment with a near complete overlap between the present study and the three-dimensional OS equation for the transverse profiles of u', v', and w'. With confidence in the model accuracy, it is now ready for investigation of turbulence transition.

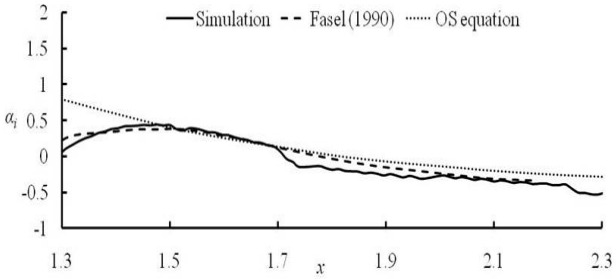

Fig. 3. Comparison of model, three-dimensional OS equation, and Fasel, *et al.*, 1990 [25] for downstream amplification rate α_i of u'.

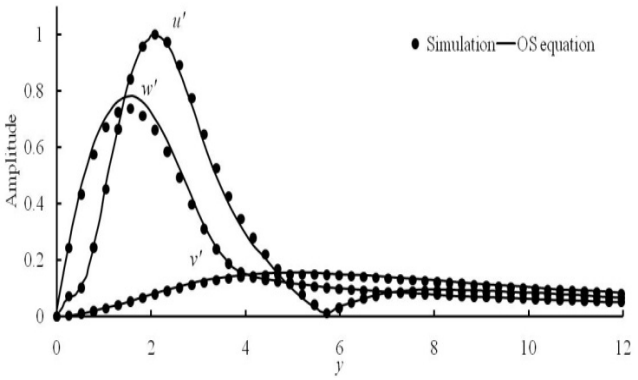

Fig. 4. Comparison of model results and three-dimensional OS equation for transverse profiles of disturbance velocities $u', v',$ and w'.

IX. Sub-Harmonic Resonance

The classical works Kachanov and Levchenko, 1984 [5] and Kachanov, 1994 [6] reveal the N-type turbulence transition involving sub-harmonic resonance of the propagating waves in ZPG boundary layer flow. The present study respectfully simulates the experiments presented forth in Kachanov and Levchenko, 1984 [5] using three Fourier modes in the spectral method with lowest wave number 31.47. The blowing and suction strip generates two-dimensional disturbances with β_0 = 12.4 and A_0 = 1.2 × 10^{-4} and three-dimensional disturbances with β_1 = 6.2 and A_1 = 5.1 × 10^{-6}.

Figure 5 shows comparison amongst the present study, experiments of Kachanov and Levchenko, 1984 [5], and numerical study of Fasel, *et al.*, 1990 [25] for downstream amplification of waves: mode (1, 0) two-dimensional initial TS waves and mode (1/2, 1) subsequently generated three-dimensional sub-harmonic waves. The first entry in the brackets such as (1, 0) stands for multiples of the fundamental TS wave frequency, and the second entry represents multiples of the spanwise wave number. The three studies agree qualitatively. Figure 6 shows further close agreement amongst the three studies for the transverse profile of the wave amplitude for the mode (1, 0). The case for the mode (1/2, 1) in Fig. 7 displays less good agreement between the numerical studies and the experiments of Kachanov and Levchenko, 1984 [5].

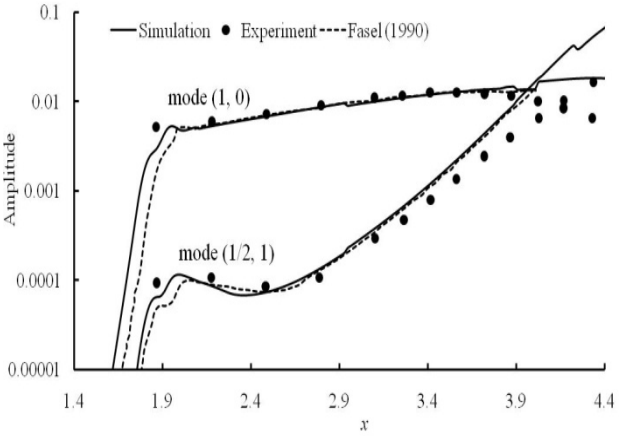

Fig. 5. Comparison amongst present study, experiments of Kachanov and Levchenko, 1984 [5], and numerical study of Fasel, *et al.*, 1990 [25] for downstream amplification of modes (1, 0) and (1/2, 1). Flow conditions given in Section III.

ISBN: 978-988-19251-9-0
ISSN: 2078-0958 (Print); ISSN: 2078-0966 (Online)

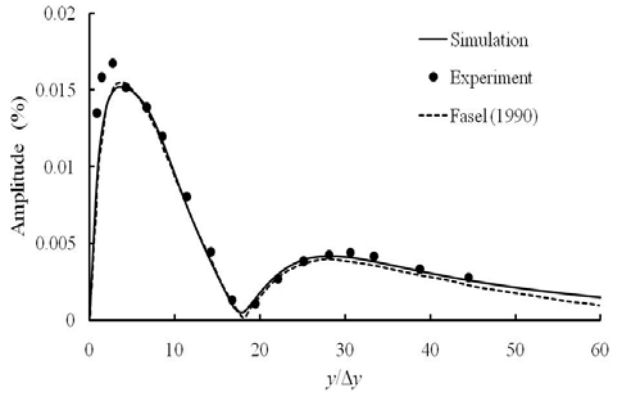

Fig. 6. Comparison amongst present study, experiments of Kachanov and Levchenko, 1984 [5], and numerical study of Fasel, *et al.*, 1990 [25] for transverse profiles of wave amplitudes of the mode (1, 0).

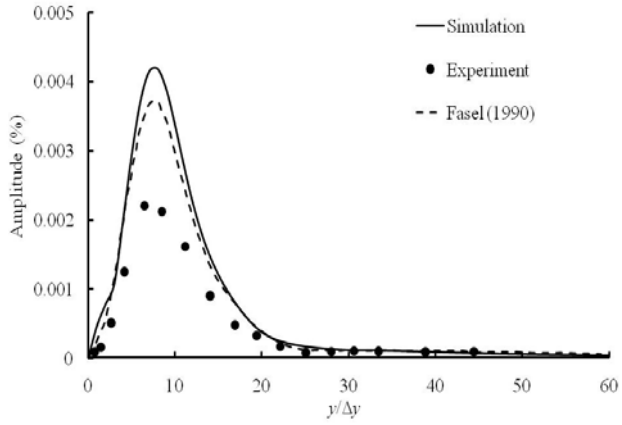

Fig. 7. Comparison amongst present study, experiments of Kachanov and Levchenko, 1984 [5], and numerical study of Fasel, *et al.*, 1990 [25] for transverse profiles of wave amplitudes of the mode (1/2, 1).

X. Conclusion

This has been a study of sub-harmonic resonance in three-dimensional ZPG boundary layer flow. Sub-harmonic wave generation, amplification, and interaction drive the N-type pathway in turbulence transition made famous by the classical works of Kachanov and Levchenko, 1984 [5] and Kachanov, 1994 [6]. At the onset of turbulence transition, the wave dynamics become three-dimensional. Investigation of three-dimensional flows propels the forefront of cutting-edge fluid dynamics research at the present time. Three-dimensionality incurs exorbitant computational demands on the numerical simulations that exponentially increase to impractical levels. The present study countervails such onerous computational demands by the imposition of a spectral method and a non-uniform grid. The symmetrical characteristic of the flow in the present study further improves upon the computational efficiency by needing only sine and cosine expansions in the spectral method, thereby reducing the computational demands by half. The non-uniform grid raises numerical stability issues at the wall boundary. Eigenvalue analysis ascertains ranges of stability of the numerical method. Validation of the numerical method versus the three-dimensional OS equation avers confidence in the accuracy of the model. The present study respectfully emulates the classical experiments of Kachanov and Levchenko, 1984 [5]. The present study realizes the resonance of the two-dimensional initial TS waves and the subsequently generated three-dimensional sub-harmonic waves with qualitative agreement to Kachanov and Levchenko, 1984 [5].

References

[1] G. Schubauer and H. K. Skramstad, "Laminar boundary layer oscillations and stability of laminar flow," *J. Aeronaut. Sci.*, vol. 14, no. 2, pp. 69-78, 1947.

[2] J. Chen and W. Chen, "Turbulence transition in two-dimensional boundary layer flow: Linear instability," in *Proc. 6th Intl. Conf. Flow Dyn.*, Sendai, Japan, 2009, pp. 148-149.

[3] J. Chen and W. Chen, "The complex nature of turbulence transition in boundary layer flow over a flat surface," *Intl. J. Emerg. Multidiscip. Fluid Sci.*, vol. 2, no. 2-3, pp. 183-203, 2010.

[4] P. S. Klebanoff, K. D. Tidstrom and L. M. Sargent, "The three-dimensional nature of boundary-layer instability," *J. Fluid Mech.*, vol. 12, no. 1, pp. 1-34, 1962.

[5] Y. S. Kachanov and V. Y. Levchenko, "The resonant interaction of disturbances at laminar-turbulent transition in a boundary layer," *J. Fluid Mech.*, vol. 138, pp. 209-247, 1984.

[6] Y. S. Kachanov, "Physical mechanisms of laminar-boundary-layer transition," *Annu. Rev. Fluid Mech.*, vol. 26, pp. 411-482, 1994.

[7] T. Herbert, "Secondary instability of boundary layers," *Annu. Rev. Fluid Mech.*, vol. 20, pp. 487-526, 1988.

[8] J. Chen, "The law of multi-scale turbulence," *Intl. J. Emerg. Multidiscip. Fluid Sci.*, vol. 1, no. 3, pp. 165-179, 2009.

[9] W. Chen and J. Chen, "Combined compact difference methods for solving the incompressible Navier-Stokes equations," *Intl. J. Numer. Methods Fluids*, in press.

[10] J. Chen and W. Chen, "Two-dimensional nonlinear wave dynamics in blasius boundary layer flow using combined compact difference methods," *IAENG Intl. J. Appl. Math.*, vol. 41, no. 2, pp. 162-171, 2011.

[11] W. Chen and J. Chen, "Spectral method and non-uniform grid for solving the incompressible Navier-Stokes equations", in preparation.

[12] J. Chen and W. Chen, "Nonlinear wave dynamics in two-dimensional boundary layer flow", *IAENG Trans. Eng. Technol. Vol. 7 - Special Ed. Intl. MultiConf. Eng. Comp. Sci.*, Hong Kong: World Scientific, in press.

[13] J. Chen and W. Chen, "Combined compact difference method for simulation of nonlinear wave generation, interaction, and amplification in boundary layer turbulence transition," in *Proc. 7th Intl. Conf. Flow Dyn.*, Sendai, Japan, 2010, pp. 82-83.

[14] J. Chen and W. Chen, "Numerical realization of nonlinear wave dynamics in turbulence transition using Combined Compact Difference methods," in *Lect. Notes Eng. Comp. Sci.: Proc. Intl. MultiConference Eng. Comp. Sci.*, Hong Kong, 2011, pp. 1517-1522.

[15] J. Chen and W. Chen, "Non-uniform grids in numerical simulations of boundary layer turbulence transition," in *Proc. 8th Intl. Conf. Flow Dyn.*, Sendai, Japan, 2011, in press.

[16] W. S. Saric, H. L. Reed and E. B. White, "Stability and transition of three-dimensional boundary layers," *Annu. Rev. Fluid Mech.*, vol. 35, pp. 413-440, 2003.

[17] S. A. Orszag and A. T. Patera, "Secondary instability of wall-bounded shear flows," *J. Fluid Mech.*, vol. 128, pp. 347-385, 1983.

[18] H. L. Reed and W. S. Saric, "Stability of three-dimensional boundary layers," *Annu. Rev. Fluid Mech.*, vol. 21, pp. 235-284, 1989.

[19] H. L. Meitz and H. F. Fasel, "A compact-difference scheme for the Navier-Stokes equations in vorticity-velocity formulation," *J. Comput. Phys.*, vol. 157, no. 1, pp. 371-403, 2000.

[20] U. Rist and H. Fasel, "Direct numerical simulation of controlled transition in a flat-plate boundary layer," *J. Fluid Mech.*, vol. 298, pp. 211-248, 1995.

[21] C. Canuto, M. Y. Hussaini, A. Quarteroni and T. A. Zang, *Spectral methods: Fundamentals in single domains,* Berlin, Heidelberg: Springer-Verlag, 2006.

[22] C. Liu and S. A. Maslowe, "A numerical investigation of resonant interactions in adverse-pressure-gradient boundary layers," *J. Fluid Mech.*, vol. 378, pp. 269-289, 1999.

[23] X. Zhong and M. Tatineni, "High-order non-uniform grid schemes for numerical simulation of hypersonic boundary-layer stability and transition," *J. Comput. Phys.*, vol. 190, no. 2, pp. 419-458, 2003.

[24] C. Hirsch, *Numerical computation of internal and external flows: Fundamentals of computational fluid dynamics, 2nd edition*. London: Butterworth-Heinemann, 2007.

[25] H. Fasel, U. Rist, and U. Konzelmann, "Numerical investigation of the three-dimensional development in boundary-layer transition," *AIAA J.*, vol. 28, no. 1, pp. 29-37, 1990.

ISBN: 978-988-19251-9-0
ISSN: 2078-0958 (Print); ISSN: 2078-0966 (Online)